Investigation of Novel Nano-carbide WC/CoCr Coatings Applied by HVAF

K. Bobzin[1] · W. Wietheger[1] · E. Burbaum[1] · L. M. Johann[1] · L. J. Rempe[1] ·
V. Matikainen[2] · U. Kanerva[2] · M. Karhu[3] · J. Lagerbom[3] · K. Kaunisto[3] ·
J.-F. Lartigue[4]

Abstract Wear leads to high material and energy losses in various industries. The manufacturing of novel nano-carbide WC/CoCr powder feedstock materials promises a further increase in the performance of thermally sprayed wear protection coatings. A novel experimental powder and a commercial ultra-fine carbide WC/CoCr reference are thermally sprayed onto a 1.0038 substrate by High Velocity Air Fuel (HVAF) spraying. The specimens are metallographically prepared and analyzed by means of light microscopy (LM) and scanning electron microscopy (SEM). Vickers Hardness testing is conducted by micro-indentation, and the porosities are determined by optical image analysis. X-ray diffractometry (XRD) analysis is used to investigate the phase retention. Fine nanocrystalline WC structures are preserved in the dense coatings. A significant effect of powder type on the porosity of the coating was found. No systematic relationships could be identified between the coating structure and the two parameter settings. It was possible to influence decarburization via both the powder type and the selected parameters. The resulting experimental and commercial nanostructured WC/CoCr coatings exhibit high, narrow hardness values with medians of $1.400 < \mathrm{HV}0.3 < 1.470$. The novel nanostructured coating can contribute to reduced wear and therefore improve the efficient utilization of critical raw materials like tungsten.

Keywords carbides · chrome replacement · HVAF · nanomaterials · WC-Co-Cr

✉ L. M. Johann
johann@iot.rwth-aachen.de

1 Surface Engineering Institute (IOT), RWTH Aachen University, Aachen, NRW, Germany

2 Valmet Technologies, Inc., Jyväskylä, Finland

3 VTT Technical Research Centre of Finland Ltd, Tampere, Finland

4 Umicore Specialty Powders France, Grenoble, France

Introduction

Thermally sprayed WC/CoCr cemented carbide coatings are a well-established form of wear protection in many industrial applications. In the production of WC/CoCr coatings by thermal spraying, the required raw materials are a significant cost factor. Tungsten carbide powders are predominantly obtained from tungsten metal powders. Increased price and supply risks are forecast for tungsten in a 2014 raw material risk assessment by the German Raw Materials Agency (DERA) (Ref 1). A study conducted by DERA in 2018 came to the same conclusion in regard to cobalt (Ref 2). For these reasons, the need for new resource-saving material concepts is growing. The use of more wear-resistant coatings with a longer service life would provide a possible solution for these challenges. Other concepts to tackle this issue include the substitution of WC or Co by other hard phases and binders. This does,

however, in many cases come at a cost of coating performance, e.g., higher wear rates of the substitute coatings. A work by Bobzin et al. (Ref 3) conducted experiments on the wear performance of HVOF sprayed WC/Co and Cr_3C_2/NiCr coatings. After pin on disk tests against an Al_2O_3 counter body, the wear rate of the Cr_3C_2/NiCr coating was about 100 times higher than the WC/Co system.

Generally, a decrease in carbide size leads to an increase in hardness and a decrease in fracture toughness in cemented carbides (Ref 4). Both hardness and fracture toughness are important factors influencing the wear behavior of a tribological system. In the recent past, a focus of research was put on the development of sub-micron and ultra-fine carbide WC/Co-based wear-resistant coatings. In many cases, authors state that due to the small carbide size, higher hardness values can be realized in such coating systems than in coatings with coarser carbides while maintaining sufficiently high resistance to crack propagation and brittle fracture (Ref 5-7). In addition, the small carbide size has other positive influences on the tribological system. For example, Yang et al. (Ref 8) indicate a positive influence on the wear mechanism in sliding wear. The corresponding tribological investigations were carried out using an Al_2O_3 counter-body. According to Al-Mutairi et al. (Ref 9), a critical factor in the fabrication of nanostructured WC/Co-based coatings is their high-volume specific surface area, which leads to a higher extent of thermally induced phase transformations in the form of decarburization. During decarburization, the oxidation and high-temperature decomposition of tungsten carbide result in a lower carbon content as well as WC phase content in the coating compared to the feedstock. Decarburization leads to the formation of W_2C and complex η-carbides, e.g., Co_3W_3C, as well as amorphization and embrittlement of the binder matrix in accordance with numerous references (Ref 9-11). Various studies have reported a negative influence of the phases formed by decarburization on the fracture toughness and tribological properties of the coating (Ref 12, 13). With the aim of minimizing carbide growth and decarburization during the production of WC/Co-based feedstock materials, a novel manufacturing route using water-soluble raw materials has been developed in the recent past (Ref 14). The experimental powder presented in this paper is a result of this effort.

WC/CoCr coatings are commonly applied by High Velocity Oxygen Fuel spraying (HVOF). Compared to, e.g., plasma spraying processes, the relatively low particle temperatures and high particle velocities in HVOF result in coatings with lower decarburization and an increased coating density. The high velocity air fuel spraying (HVAF) process is a new complementary variant to the HVOF process. While the HVOF process uses pure oxygen as the oxidant for combustion, the HVAF process uses compressed air. According to Jacobs et al. (Ref 15), compared to the HVOF process, the HVAF process provides an even lower degree of oxidation and decomposition during the application of WC/Co-based coatings. As the works of Bobzin and Verstak et al. (Ref 16, 17) also conclude, in comparison with HVOF spraying, HVAF spraying of hardmetals offers a considerably lower degree of oxidation and decarburization of the feedstock at porosities of less than 1%. While the HVAF spraying of conventional hard metals has drawn some attention in the literature, still far fewer publications in comparison with HVOF spraying of conventional WC/Co feedstock can be found. Consequently, the literature on HVAF spraying of nanostructured WC/Co feedstock is even more scarce. Since the HVAF process appears to be suitable for the processing of nanostructured WC/Co, it is investigated in this work. The overall aim of the present work is the manufacturing of dense coatings with a high WC phase retention.

Experimental Procedure

Feedstock Materials

In this work, an experimental 80WC/14Co6Cr powder with carbide sizes in the nano-scale of $\varnothing_{WC} \approx 50$ nm is investigated. For the synthesis of this powder, a new manufacturing route using water-soluble raw materials was used, as reported by Karhu et al. (Ref 14). Since the experimental powder contains Cr_3C_2, the WC content was slightly lowered in order to ensure good manufacturability. For a reference feedstock, the commercial 86WC/10Co4Cr powder Amperit 507.059 from Höganäs (Düsseldorf, Germany) is chosen. The carbide sizes in this commercial powder extend into the ultra-fine scale of $\varnothing_{WC} \approx 200$-400 nm with a particle size distribution of $d10/d50/d90 = 11$ μm/18 μm/29 μm and an apparent bulk density of $\rho = 5.8$ g/cm^3.

HVAF Spraying

The substrates used for HVAF spraying are made of unalloyed structural steel (1.0038) and are cut to dimensions of $120 \times 50 \times 8$ mm^3. Before spraying, all substrates are grit-blasted with corundum F16 at a pressure of $p = 0.6$ MPa and then cleaned with ethanol and compressed air. An AK-07 spray gun from Kermetico Inc., Benicia, California, USA, is used for thermal spraying. Propane and compressed air are used as fuel and oxidant, respectively. A Laval nozzle with a high length of $l = 275$ mm is used. Since the open jet is eventually slowing down, higher particle velocities can be achieved

compared to shorter nozzles when the distance between combustion chamber and substrate is kept constant. With the goal of a coating thickness of $s = 150$ μm, three repetitions with ten passes per repetition are carried out for each sample. Between the individual repetition, the samples are cooled to $T < 50$ °C with compressed air.

The parameters used are listed in Table 1. With parameter set 0, promising results have already been obtained in (Ref 16) for HVAF spraying of conventional 86WC/10Co4Cr coatings on the same equipment. For parameter set 1, a comparable spray distance is used. With the aim of increasing the productivity of the spraying process, compared to parameter set 0, the robot speed is increased from $v_0 = 900$ mm/s to $v_1 = 1,000$ mm/s and the powder feed rate from $m_0 = 40$ g/min to $m_1 = 50$ g/min. Previous experience showed that these changes have no significant effect on the coating quality. Since the hydrogen flow affects the particle temperature, it is assumed that higher hydrogen flows result in a more pronounced decarburization. Compared to the study conducted in (Ref 16), finer carbides are used in this work. The increased volume-specific surface area of the carbides leads to a higher susceptibility for decarburization. For parameter set 1, the hydrogen flow is therefore reduced from $HF_0 = 41$ SLPM to $HF_1 = 12$ SLPM, in order to realize a lower heat input into the particles during the process.

Powder and Coating Characterization

As preparation for the investigations, cross sections were cut out of the coated specimens using a precision cutting machine. The cross sections were then hot-embedded in epoxy resin and prepared by grinding and polishing. Final polishing was performed with a 1-μm diamond suspension.

To investigate the coating structure and thickness, optical microscope images with $200 \times$ magnification were taken of the metallographically prepared cross sections. The open-source software ImageJ is used for image processing and determination of the coating thickness and porosity. The porosity was determined using a stitched image of the dimensions $A_{stitch} = 5,000 \times 100$ μm^2. Objects with an area A of 1 μm$^2 \leq A \leq 50$ μm^2 are included in the measurement. Smaller or larger objects are assigned to other components such as impurities or artifacts by sample preparation. To determine the coating thickness, 10 individual measurements were taken at a distance of $d \geq 500$ μm and averaged. Furthermore, the morphology of the powders and the coating structure of the cross sections were analyzed by scanning electron microscope (SEM) using backscattered electrons (BSE). The micro-Vickers hardness was determined in the cross sections with a load of $m = 300$ g at an indentation time of $t = 15$ s. The indentation load of $m = 300$ g ensures an adequate distance of indented area to surface and interface, respectively. The hardness values reported are based on $n = 30$ individual measurements. The phases contained in the coatings were examined by x-ray diffraction (XRD) in a range from $20° \leq 2\theta \leq 80°$ using a Cu-K$_\alpha$ radiation source. For that purpose, an XRD 3000 by GE Energy Germany, Ratingen, Germany, was employed. For the phase recognition, pdf cards from the pdf-2 software by ICDD, Philadelphia, USA, were available.

Table 1 Overview of the parameters for HVAF process, chemical composition and nomenclature of the examined samples

Parameter	Unit	Parameter set	
		0	1
Stand-off distance	mm	175	180
Robot velocity	mm/s	900	1,000
Propane pressure	bar	5.55	5.55
Air pressure	bar	6.28	6.28
Nitrogen flow	SLPM	18	18
Hydrogen flow	SLPM	41	12
Powder feed	g/min	40	50

Powder	Chemical composition	Particle size distribution $d10/d90$, μm	Apparent density, g/cm^3	Parameter set	
				0	1
Chemical composition and nomenclature					
VTT-experimental	80WC/14Co6Cr	12.1/43.3	4.0	Exp0	Exp1
Amperit 507.059	86WC/10Co4Cr	11.0/29.0	5.8	Amp0	Amp1

Fig. 1 BSE-SEM analysis of the experimental 80WC/14Co6Cr nano-carbide powder on the left and the commercial ultrafine 86WC/10Co4Cr carbide powder on the right side
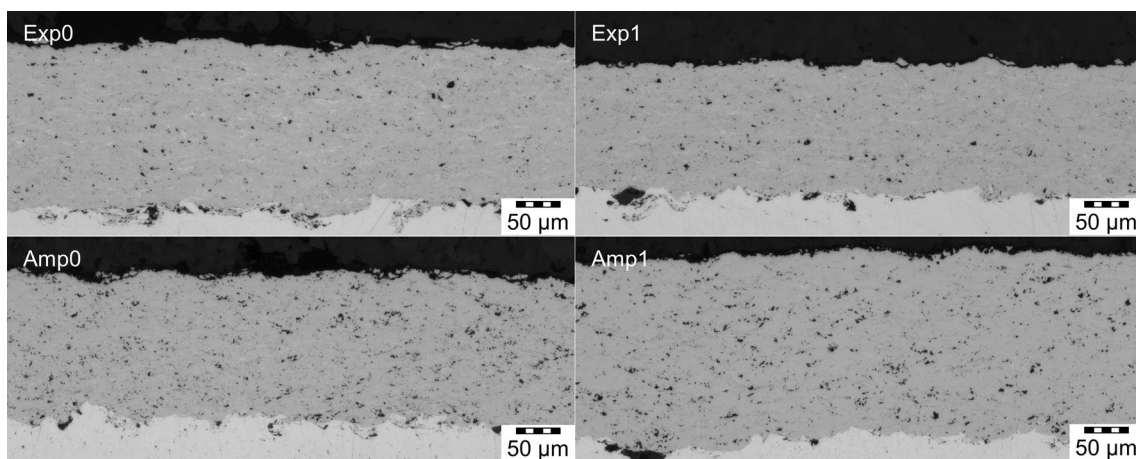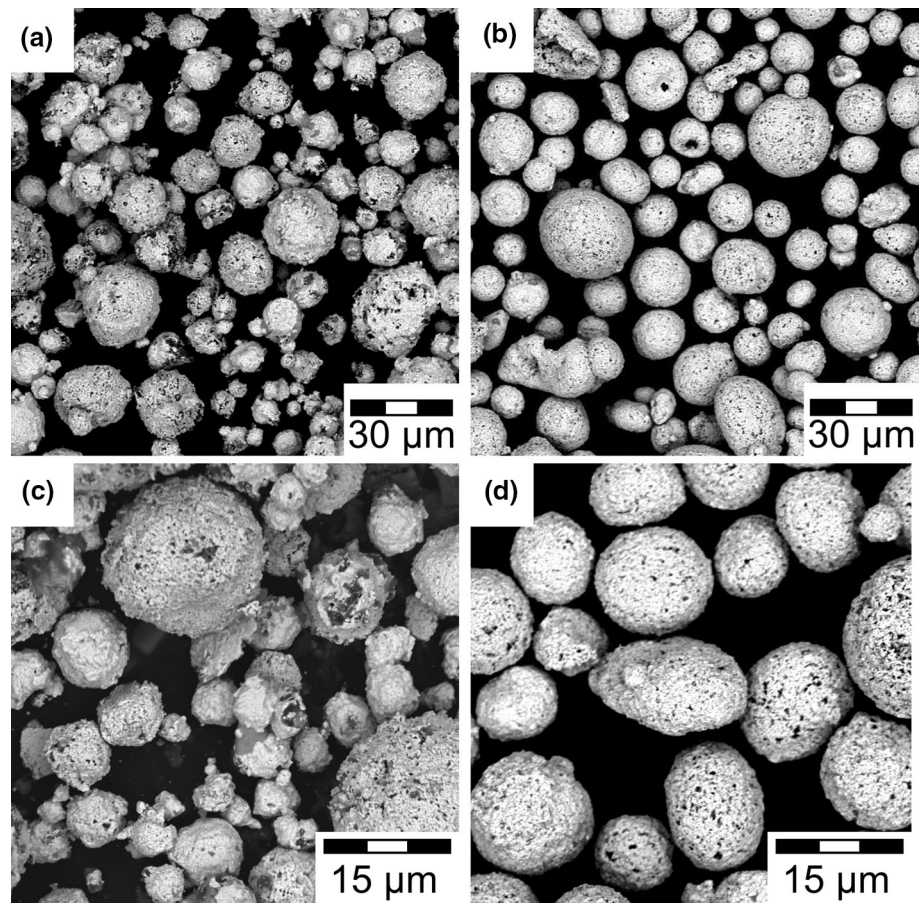

Fig. 2 Optical microscopic images of the coatings applied by HVAF using the experimental 80WC/14Co6Cr nano-carbide powder for Exp0 and Exp1 and the commercial ultra-fine 86WC/10Co4Cr carbide powder for Amp0 and Amp1

Results and Discussion

Characterization of the Spray Powders

Figure 1 shows SEM images of the two powders at 2,000 × magnification. Figure 1(a) shows the experimental powder, Fig. 1(b) the commercial reference. The experimental powder exhibits an approximately spherical shape with an irregular surface. For the fabrication of the reference powder, agglomeration and sintering were used, which resulted in a spherical powder morphology typical for this production route. Compared to the reference powder, the open porosity varies more between the individual particles of the experimental powder. Large open

pores in the experimental feedstock become evident when comparing Fig. 1(c) and (d). This observation is in line with the apparent densities in Table 1. In addition to that, there is a higher amount of smaller particles in the experimental powder. Some finer particles with a diameter $d < 2$ µm adhere to the larger sintered particles. A sintering neck between those particles can be identified in Fig. 1(c). The proportion of loose fine particles in the experimental powder can be easily removed by further post-processing steps, e.g., sieving, if necessary.

Coating Structure and Coating Thickness

Figure 2 shows optical micrographs of the cross sections of the specimens. For both parameter sets, the coating prepared with the experimental powder exhibits a significantly

Table 2 Coating thickness and porosity of the coatings applied by HVAF using the experimental 80WC/14Co6Cr nano-carbide powder for Exp0 and Exp1 and the commercial ultra-fine 86WC/10Co4Cr carbide powder for Amp0 and Amp1

Specimen	Coating thickness, µm	Porosity, %
Exp0	164 ± 11	0.5
Exp1	143 ± 5	0.4
Amp0	152 ± 6	1.8
Amp1	163 ± 15	1.9

lower porosity. A significant influence of the different parameter sets on the porosity cannot be identified by quantitative analysis with Image J. Challenges in the porosity measurement apart from the measurement error are defects such as cross section breakouts during preparation as well as the subjectivity of the commonly used grayscale thresholding method. The first does especially hold true for brittle materials such as the hard metal feedstock used in this work. Even within standardized procedures (Ref 18), there is significant margin of error.

The values for the coating thickness and porosity are summarized in Table 2. The coating thicknesses are in a similar range for all samples. Significant influences of the different parameter sets or the powder type on the coating thickness cannot be identified. Generally, a difference in coating things and porosity would imply a difference in deposition efficiency due to the parameter set or feedstock used. However, in this work, the specimen is well within standard deviations, i.e., even for higher coating thicknesses or lower porosities no significant conclusion can be drawn.

Figure 3 shows SEM images of the coatings at 20,000 × magnification. The WC particles appear bright, while the metallic co-matrix shows different gray tones. According to Jacobs et al. (Ref 15), the different shades of gray result from locally different chemical compositions of the binder matrix. Lighter shades of gray indicate that a higher proportion of the heavy element W is dissolved in

Fig. 3 BSE-SEM analysis of the coatings applied by HVAF using the experimental 80WC/14Co6Cr nano-carbide powder for Exp0 and Exp1 and the commercial ultra-fine 86WC/10Co4Cr carbide powder for Amp0 and Amp1
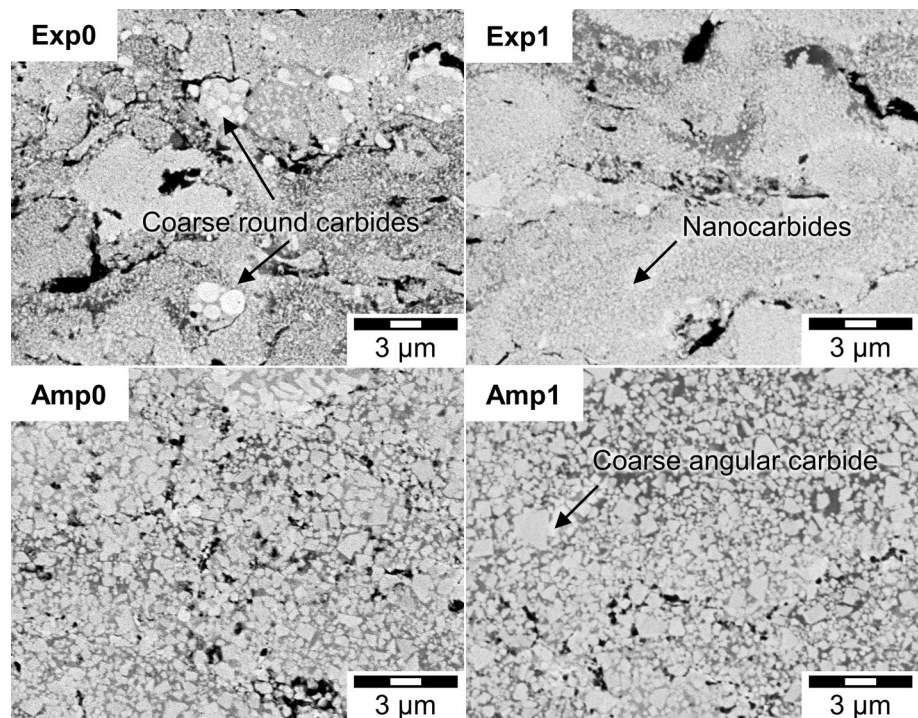
the matrix. Darker areas indicate a high proportion of the lighter elements Co and Cr. The appearance of W_2C is manifested by halos around the WC particles. These halos are even brighter than the WC because they are richer in the heavy element W.

The deviating gray tones of the binder matrix in Fig. 3 and brighter areas around the WC particles thus indicate that some decarburization has occurred. The carbide sizes of samples Exp0 and Exp1 are mainly in the range of a few nanometers. Locally, strong deviations from these small carbide sizes occur. For sample Amp0 and Amp1, the carbide sizes reach from the sub-micron to the ultra-fine range. The carbides in the reference coatings exhibit an irregular and angular morphology. This indicates the WC used here was crushed or milled down to the desired size. The WC in the experimental powder, to the contrary, forms roundly shaped carbides due to the chemical synthesis route. The microstructures are dominated by areas of nanoscaled WC particles. As Karhu et al. (Ref 14) have concluded for this manufacturing route, the carbide size herein is in a range of $10\ nm < d_{WC}\ 100\ nm$. Some local variations in carbide content, i.e., coarse grains can be observed in samples Exp0 and Exp1.

Phase Analysis

Figure 4 shows the diffractograms of the four samples and both feedstock powders. The dashed vertical lines indicate the position of the main reference peaks of the pure phases. For improved visualization, only reference peaks with an intensity above $I = 10\%$ are plotted as dashed vertical lines. Comparing the samples to the feedstock powder reveals a difference in α-Co phase. The Co(Cr) peak is more pronounced for the experimental powder. After processing the portion of α-Co is not significant anymore. Some α-Co has reacted to form η-carbides of the Co_3W_3C type. These could not be detected in either feedstock

powder. Apart from that, the samples are mainly composed of WC, which is clear from the large peaks at $2\theta \approx 48°$ (48.3° according to reference), $2\theta \approx 35.5°$ (35.6°) and $2\theta \approx 31.5°$ (31.5°). The peak at $2\theta \approx 40°$ lies between the main intensity peaks of the W_2C and W phases and thus probably represents an overlapping peak of these two phases. Compared with the WC peaks, this overlapped peak has a low height. The height of the peaks is not equivalent to the quantitative fraction of the respective phase. However, a qualitative assessment of the phase proportions based on the height of the peaks is possible. Accordingly, the low peak at $2\theta \approx 40°$ indicates that a small fraction of decarburization phases is present. This decarburization peak is more pronounced for parameter set 0 than for parameter set 1. In addition, it can be seen that slightly higher decarburization occurred for the samples obtained from the experimental powder.

In the magnified view on the right of Fig. 4, these differences can be observed. Especially in the coating Exp0 slightly higher formation of decarburization products can be noted. Hence, Amp0 exhibited the lowest degree of decarburization. Nevertheless, the overall differences between the diffractograms are small.

Hardness of the Coatings

Figure 5 shows a boxplot of the hardness values determined for the samples. Overall, the individual measurements are in a similar range, although slightly increased hardness values can be achieved with the reference coatings. The averaged microhardness of the specimens prepared from the experimental powders Exp0 is $1,414 \pm 70$ HV0.3 and Exp 1 $1,383 \pm 87$ HV0.3, that of the reference specimens with Amp0 is $1,460 \pm 103$ HV0.3 and for Amp1 $1,427 \pm 74$ HV0.3. The averaged hardness values of Exp0 and Exp1 are thus slightly lower than those of Amp0 and Amp1, but still lie in a comparable range. A
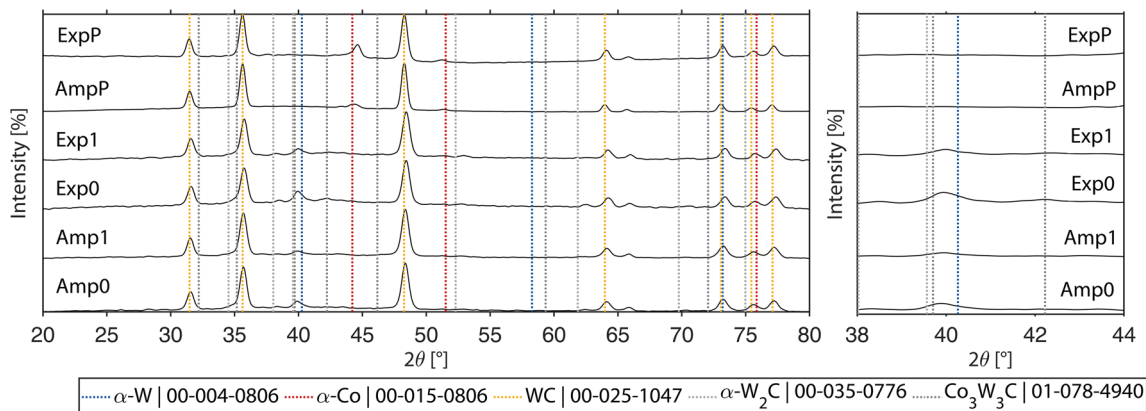

Fig. 4 X-ray diffraction analysis of the experimental 80WC/14Co6Cr nano-carbide powder ExpP, the commercial ultra-fine 86WC/10Co4Cr carbide powder AmpP and the corresponding coatings applied by HVAF at different parameter sets for Exp0, Exp1, Amp0, Amp1
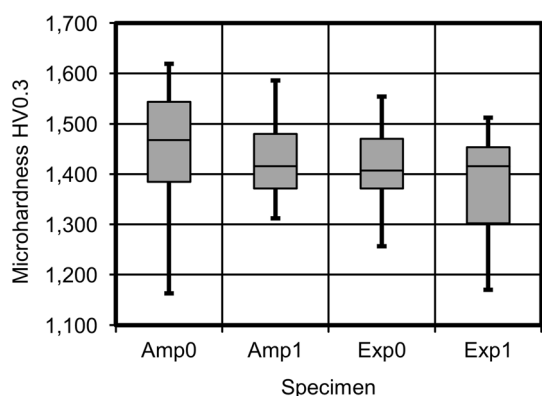
Fig. 5 Boxplot representation of the hardness values of the coatings applied by HVAF using the experimental 80WC/14Co6Cr nanocarbide powder for Exp0 and Exp1 and the commercial ultra-fine 86WC/10Co4Cr carbide powder for Amp0 and Amp1

possible reason for the slightly lower hardness of the experimental 80WC/14Co6Cr powder compared to the commercial 86WC/10Co4Cr powder is the lower WC content.

As expected, an increased standard deviation can be observed due to the high overall hardness. In addition to that the thermal spray process yields an inhomogeneous microstructure which is very much dominated a lamella structure and splat boundaries. The inhomogeneities that originate from the spraying process too, result in an increased measurement scatter. An in-depth investigation of processing and wear behavior of HVOF and HVAF sprayed commercial WC/CoCr feedstock was conducted by Bocelli et al. (Ref 19). Therein, a median Vickers hardness of HV0.3 < 1.250 or less was measured for the HVAF sprayed coatings. The significantly higher hardness observed in the present work is expected to result from the nanostructured feedstock powder.

Conclusions

It has been demonstrated that the experimental WC/CoCr powder has the potential to substitute currently used commercial powders. The investigated coating properties of Exp0 and Exp1 are comparable to those of Amp0 and Amp1 or exceed them.

The results can be summarized as follows:

- For both powders, successful coating application was possible with the selected parameter sets.
- The coatings produced from the experimental WC/CoCr powder exhibited lower porosity than the reference coatings, with comparable hardness and coating thickness.

- The majority of the carbides in the coatings produced from the experimental powder have a size in the range of a few nanometers and are thus far smaller than the carbides in the reference coating. The homogeneity of the Exp0 and Exp1 coatings is reduced by local deviations in carbide size and content.
- The XRD measurement results suggest that a small number of decarburization-formed phases are present in all coatings. The diffractograms suggest a slightly higher decarburization for the experimental powder.

Verification of the reproducibility of the results made in this study is still ongoing. Future work includes the manufacturing of bimodal WC/CoCr by mixing the nanostructured powders with conventional micron-scale carbide WC/CoCr, as well as investigations of the tribological properties of the coating. If the higher decarburization in the experimental powder has a significant impact on the tribological properties, the development of an optimized parameter set for an even lower decarburization is needed. In addition, the influence of the local variations in carbide size and content on the tribological properties should be investigated.

References

1. M. Liedtke and M. Schmidt, *Rohstoffrisikobewertung-Wolfram*, 1st ed. Deutsche Rohstoffagentur, Berlin, Germany, 2014.

2. S.A. Barazi, *Rohstoffrisikobewertung-Kobalt*, 2018th ed. DERA, Berlin, Germany, 2018.

3. K. Bobzin, W. Wietheger, H. Heinemann, M. Schulz, M. Oechsner, T. Engler, H. Scheerer, and Y. Joung, Thermally Sprayed Coatings For the Valve Industry, *Mat. wiss. u. Werkstofftech.*, 2021, **52**(9), p 997-1011.

4. V.K. Sarin, D. Mari, and Llanes, Luis (Hrsg.), (eds.), Hardmetals, (Elsevier, 2014) Ref. (in eng)

5. C. Bartuli, T. Valente, F. Cipri, E. Bemporad, and M. Tului, Parametric Study of an HVOF Process For the Deposition of Nanostructured Wc-Co Coatings, *J. Therm. Spray Technol.*, 2005, **14**(2), p 187-195.

6. A. Lekatou, D. Sioulas, A.E. Karantzalis, and D. Grimanelis, A Comparative Study on the Microstructure and Surface Property Evaluation of Coatings Produced from Nanostructured and Conventional Wc–Co Powders HVOF-Sprayed on Al7075, *Surf. Coat. Technol.*, 2015, **276**, p 539-556.

7. F. Zishuan, W. Shansong, and Z. Zhengdong, Microstructures and Properties of Nano-Structural Wc-12Co Coatings Deposited By Ac-HVAF, *Rare Metal Mater. Eng.*, 2017, **46**(4), p 923-927.

8. Q. Yang, T. Senda, and A. Ohmori, Effect of Carbide Grain Size on Microstructure and Sliding Wear Behavior of Hvof-Sprayed Wc–12% Co Coatings, *Wear*, 2003, **254**(1-2), p 23-34.

9. S. Al-Mutairi, M. Hashmi, B.S. Yilbas, and J. Stokes, Microstructural Characterization of Hvof/Plasma Thermal Spray of Micro/Nano Wc–12%Co Powders, *Surf. Coat. Technol.*, 2015, **264**, p 175-186.

10. R. Schwetzke and H. Kreye, Microstructure and Properties of Tungsten Carbide Coatings Sprayed With Various High-Velocity Oxygen Fuel Spray Systems, *J. Therm. Spray Tech.*, 1999, **8**(3), p 433-439.

11. D. Stewart, P. Shipway, and D. McCartney, Microstructural Evolution in Thermally Sprayed Wc–Co Coatings: Comparison Between Nanocomposite and Conventional Starting Powders, *Acta Mater.*, 2000, **48**(7), p 1593-1604.

12. D.A. Stewart, P.H. Shipway, and D.G. McCartney, Abrasive Wear Behaviour of Conventional and Nanocomposite Hvof-Sprayed Wc–Co Coatings, *Wear*, 1999, **225-229**, p 789-798.

13. E. López Cantera and B.G. Mellor, Fracture Toughness and Crack Morphologies in Eroded Wc–Co–Cr Thermally Sprayed Coatings, *Mater. Lett.*, 1998, **37**(4-5), p 201-210.

14. M. Karhu, J. Lagerbom, K. Kaunisto, T. Suhonen, J. Metsäjoki and E. Turunen, Nanocrystalline Wc–Co HVAF Coatings By Utilizing Novel Powder Manufacturing Route Using Water-Soluble Raw Materials, *J. Therm. Spray Technol.*, 2018, **27**(1-2), p 196-206.

15. L. Jacobs, M.M. Hyland, and M. de Bonte, Comparative Study of Wc-Cermet Coatings Sprayed Via the HVOF and the HVAF Process, *J. Therm. Spray Technol.*, 1998, **7**(2), p 213-218.

16. K. Bobzin, N. Kopp, T. Warda, M. Schäfer, and A. Verstak, Investigation and Characterization of HVAF Wc-Co-Cr Coatings and Comparison to Galvanic Hard Chrome Coatings, Itsc 2013: Innovative Coating Solutions For the Global Economy, Proceedings of the International Thermal Spray Conference, 13.05.-15.05.2013, Busan, Republic of Korea, R.S. Lima, A. Agarwal, M.M. Hyland, Y.-C. Lau, G. Mauer, A. McDonald, and Toma, F.-L. (Hrsg.), (eds.), (ASM International, 2013) pp 389-394

17. A. Verstak and G. Kusinski, High Velocity Air-Fuel Spraying and Its Applications in Oil and Gas Industry, Itsc 2012: Air, Land, Water and the Human Body, Proceedings of the International Thermal Spray Conference, 21.05.-24.05.2012, Houston, USA, B.R. Marple, A. Agarwal, M.M. Hyland, Y.-C. Lau, C.-J. Li, R.S. Lima, and McDonald, André (Hrsg.), Eds., (ASM International, 2012), pp. 529-534

18. Deutsches Institut für Normung, Din En Iso 4499-4:2016-10, Hartmetalle–Metallographische Bestimmung Der Mikrostruktur–Teil 4: Charakterisierung Von Porosität, Kohlenstofffehlern Und Anteil an Eta-Phase (Iso 4499-4:2016): Deutsche Fassung EN ISO 4499-4:2016 (2016)

19. G. Bolelli, L. Lusvarghi, and M. Barletta, HVOF-Sprayed Wc–Cocr Coatings on Al Alloy: Effect of the Coating Thickness on the Tribological Properties, *Wear*, 2009, **267**(5-8), p 944-953.